Finite element analysis of the piezoelectric stacked-HYBATS transducer

2013 Smart Mater. Struct. 22 035015

(http://iopscience.iop.org/0964-1726/22/3/035015)

Smart Mater. Struct. **22** (2013) 035015 (11pp) doi:10.1088/0964-1726/22/3/035015

Finite element analysis of the piezoelectric stacked-HYBATS transducer

Laura Tolliver[1], **Tian-Bing Xu**[2] **and Xiaoning Jiang**[1]

[1] Department of Mechanical and Aerospace Engineering, North Carolina State University, Raleigh, NC 27695, USA
[2] National Institute of Aerospace, 100 Exploration Way, Hampton, VA 23666, USA

E-mail: xjiang5@ncsu.edu

Received 8 December 2012, in final form 18 January 2013
Published 14 February 2013
Online at stacks.iop.org/SMS/22/035015

Abstract
Finite element modeling (FEM) of a piezoelectric multilayer-stacked hybrid actuation/transduction system (stacked-HYBATS) is investigated in this paper using ANSYS software. This transducer consists of two positive strain components operating in d_{33} mode and one negative strain component operating in d_{31} mode to generate large displacements. FEM results are compared with experimental and analytical results to provide insight into the actuation mechanisms, verify the device's three displacement components, and estimate its blocking force. FEM calculations found the effective piezoelectric coefficient to be exceptional, about 3.11×10^6 pm V^{-1} at resonance. Stacked-HYBATS was quantitatively compared to commercially available flextensional actuators using finite element analysis. It was found that under the same electric field the yielded displacement of a stacked-HYBATS is about 200% and 15% larger than that of a same-sized d_{31} and d_{33} flextensional actuator, respectively. These findings suggest that stacked-HYBATS is promising for precision positioning, vibration control, and acoustic applications.

(Some figures may appear in colour only in the online journal)

1. Introduction

Piezoelectric transduction structures have been exploited in a variety of high value applications including acoustics, sensing, energy harvesting, and actuation. For example, hydrophones are used in the military and biomedical fields for detecting underwater sound waves and calibrating the output of ultrasound devices for medical imaging and therapy [1]. Geophones have both military and civilian applications in sensing changes in rock formations and soil [2]. Other piezoelectric sensors are used as accelerometers [3], in reporting humidity, temperature, and viscosity [3], and in nondestructive testing and structural health monitoring [4]. The high power density of piezoelectrics at low voltages as well as ease in using their harvested energy has made these transducers viable substitutes for external power sources [5]. Finally, piezoelectric actuators are known to have large strains at relatively low electric fields, quick response times, large output displacements, and high generative forces [5].

Recent work in hydrophone technology and nondestructive testing has attempted to increase sensitivity as well as produce a stable output over a wide range of frequencies. Meanwhile, a variety of sensor configurations have been developed to produce the largest possible voltage response [1–3, 6, 7]. In the case of actuators, research has focused on generating the largest blocking forces and displacements at low operating voltage. In general, a piezoelectric transducer converts mechanical energy to electrical energy or vice versa; an improvement in the performance of one transducer type (e.g. an actuator) can be used to improve performance in another (e.g. a sensor). For example, an actuator with broad frequency bandwidth at resonance could also be used for broadband energy harvesting and acoustic sensing. Thus, an actuator with favorable dynamic response holds promise for the energy harvesting and sensing areas as well. To this end, this paper focuses on a novel piezoelectric actuator configuration which in turn has far-reaching implications for other piezoelectric transduction structures.

Table 1. Comparison of piezoelectric actuators compiled from a variety of sources as labeled.

Configuration	Dimensions (mm)	Active material	Amplification ratio	Max. stroke (μm)	Blocking force (N)
Cantilever [15]	$34.9 \times 12.7 \times 2.5$	PZT-5A	N/A	$\pm$1260	$\pm$0.31
Multilayer stack [16]	$25.1 \times 25.1 \times 20$	PZT-5	N/A	15.6	20 000
THUNDER [10]	$r = 2540$ $t = 0.381$	PZT-5A	N/A	375	$<$10 [17]
RAINBOW [10]	$r = 2540$ $t = 0.381$	PZT-5A	N/A	300	$<$10 [18]
Moonie	$11 \times 11 \times 3.4$ [11]	PZT-5 [11]	5 [19]	22 [11]	3 [19]
Cymbal	$12.7 \times 12.7 \times 2$ [12]	PZT [20]	40 [12]	40 [12]	20 [12]
Flextensional [21]	$13.3 \times 10 \times 5.5$	PZT	5	55	27
Flextensional [14]	$27.4 \times 13.6 \times 10$	PMN–PT single crystal	3.89	96.5	Hundreds
HYBAS [22]	$5.5 \times 3 \times 1$	[P(VDF–TrFE)], PZN–PT single crystal	2.5	$>$350	N/A
Stacked-HYBATS [23]	$35.5 \times 10 \times 18$	TRS-HK1-HD	-10	30	N/A

2. Actuation mechanism and design rationale

First, we will briefly summarize the main piezoelectric actuator configurations. This will allow us to place our device in the context of the body of research literature. The earliest example of a piezoelectric actuator is the fixed–free cantilever. This transducer is comprised of two piezoelectric plates bonded together and electrically connected in series or parallel. Commercial models of this type offer large displacements of over a millimeter but very small blocking force ($<$0.5 N) [8]. The multilayer piezoelectric stack is another actuator configuration in which many thin plates of piezoelectric ceramic are bonded together. The plates are connected in parallel electrically and the poling direction of each plate is aligned parallel to the applied electric field, so each plate expands or contracts at the same time. These stack actuators produce smaller displacements (in the range of 10–20 μm) but very large blocking force (2600 N) [9]. In order to produce both large displacements and high generative force, amplification structures have been developed. In the cases of RAINBOW and THUNDER, the amplification structure is a thin sheet of metal that is bonded to the piezoelectric material. The curved shape of the actuators produces a stress in the piezoelectric layer that causes large deformations ($\sim$375 μm) under an applied electric field [10]. In other amplified actuators a piezoelectric element is sandwiched between metal end caps or a metal frame. In these configurations a small horizontal displacement in the piezoelectric element is amplified into a much larger vertical displacement via the end caps or frame. In the moonie each metal end cap is a disk with a semi-ellipsoid solid removed; in the cymbal the metal end cap is a thinner dome-shaped structure with a flat top. These actuators have the advantage of using both the d_{31} and d_{33} piezoelectric coefficients for an enhanced amplification ratio [11, 12]. An even more popular configuration for commercial applications is the flextensional actuator which is comprised of a piezoelectric element (usually a multilayer stack or a bar) inside a metal frame. Such actuators are capable of producing large displacements and relatively large generative force. For instance, an actuator of this type having dimensions 57 mm $\times$ 214.3 mm $\times$ 21 mm can produce 1050 μm of displacement and 745 N of blocking force [13]. Additionally, the performance of such flextensional actuators can be further optimized through an appropriate choice of active material. For example, replacing the piezoelectric multilayer stack in a flextensional actuator with a single-crystal PMN–PT stack results in increased displacement [14]. A summary of the actuator types and their major performance specifications is shown in table 1.

Recently, Xu, Su, and Jiang presented two variations on the flextensional design known as HYBAS and stacked-HYBATS [22–24]. These designs contrast with those described above in that these new configurations synergistically use both the expansion and the contraction of smart materials. Each configuration contains one or more positive strain components (PSCs) as well as a negative strain component (NSC), as shown below in figure 1. The positive strain components in each device are comprised of a material that expands when a voltage is applied. This material is [P(VDF–TrFE)] (a PVDF copolymer film) and d_{33} mode piezoelectric ceramic or single crystal in HYBAS and stacked-HYBATS, respectively. Similarly, the negative strain components are comprised of a material that contracts when a voltage is applied; d_{31} mode relaxor single-crystal or piezoelectric ceramics can be used in both HYBAS and stacked-HYBATS. When the material of the negative strain component is activated and contracts along the x-direction, the positive strain components are stressed and displace in the z-direction. At the same time, if the positive strain component(s) is (are) activated, this material expands, and additional displacement in the z-direction is obtained. The combined effect brings about more vertical displacement than would be possible from using either the positive or the negative strain component alone. For example, when both

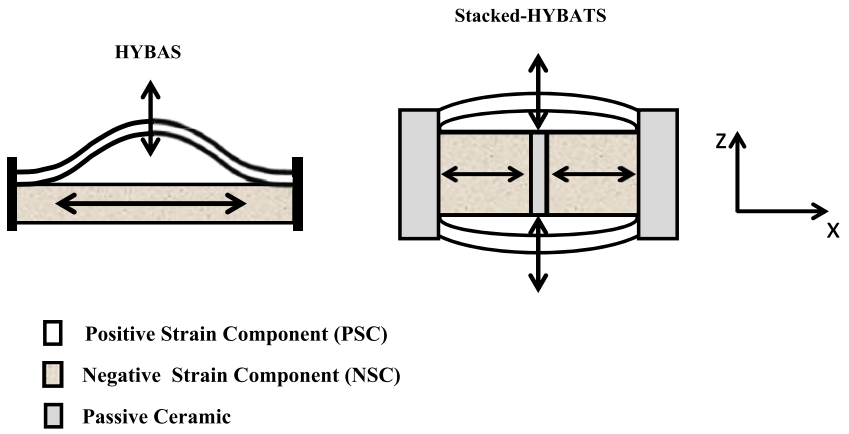

Figure 1. Cross-section of HYBAS and stacked-HYBATS. Upon actuation, the negative strain components (NSCs) in each device contract in the x-direction while the positive strain components (PSCs) bend and expand. This produces enhanced displacement in the z-direction. The arrows indicate the displacement directions.

components were activated, HYBAS featured over 225 μm of vertical displacement, while activating only the positive or negative strain component resulted in 190 μm and 75 μm of vertical displacement, respectively.

The first prototype of stacked-HYBATS featured TRS-HK1-HD in both its positive and negative strain components. This material is a high density piezoelectric ceramic with high dielectric constants. Both expansion and contraction are accessible in this material because the direction of strain (either positive or negative) is determined by the structural orientation as well as the directions of poling and electric field application. For example, the piezoelectric solid shown in figure 2 is oriented in the ⟨001⟩ direction and is poled in the z-direction. Upon application of an electric field as shown, the solid expands in the z-direction (longitudinal or d_{33} mode) and contracts in the x-direction (transverse or d_{31} mode). Similarly, when the solid contracts in the z-direction it expands in the x-direction. So, positive and negative strain are both possible in both modes as long as the appropriate structural orientation as well as poling and electric field directions are used. It is noteworthy, however, that the strain generated in the transverse direction is a little less than half that generated in the longitudinal direction. In other words, the d_{33} mode of actuation provides more displacement than the d_{31} mode. In spite of this, however, the stiffness of the TRS-HK1-HD material is almost identical in the x- and z-directions.

The novel actuation mechanism of stacked-HYBATS has been proven feasible by Xu *et al* [23]. Experimental results showed the system's viability with its large displacements, strong resonance, and large effective piezoelectric coefficient [23]. However, a discrepancy was found between the simple analytical model and the measured displacements. In this study, finite element analysis is employed to verify the measured displacements and to further understand the operation mechanism of stacked-HYBATS. In addition, this paper presents a quantitative comparison of the operating characteristics of the stacked-HYBATS, commercially available d_{33} mode flextensional actuators, and d_{31} mode flextensional actuators. Finally, we will discuss the many applications of the device for sensing, energy harvesting, and actuation.

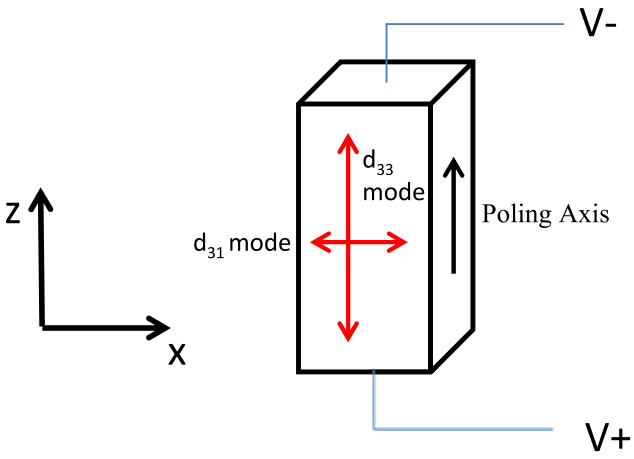

Figure 2. A piezoelectric brick poled in the z-direction with voltage applied as shown expands in the z-direction (known as longitudinal or d_{33} mode actuation) and contracts in the x-direction (known as transverse or d_{31} mode actuation).

3. Experimental and analytical results [23]

Firstly, stacked-HYBATS was fabricated with dimensions and poling directions as shown below in table 2 and figure 3. The initial shape of the positive strain components (PSCs) is given by

$$z_{\mathrm{i}}(x) = \frac{1}{\mathrm{c}}\left[\left(\frac{L}{2}\right)^2 - x^2\right]^2 \tag{1}$$

where x is the position along the x-axis, $L = 25$ mm, and $c = 47\,000$ mm^3. Additionally, the initial curvature length of the PSCs is given by

$$L^{\mathrm{i}}_{\mathrm{PSC}} = \int_{-L/2}^{L/2}\left[\left(\frac{\mathrm{d}z_{\mathrm{i}}(x)}{\mathrm{d}x}\right)^2 + (1)^2\right]^{1/2}\mathrm{d}x. \tag{2}$$

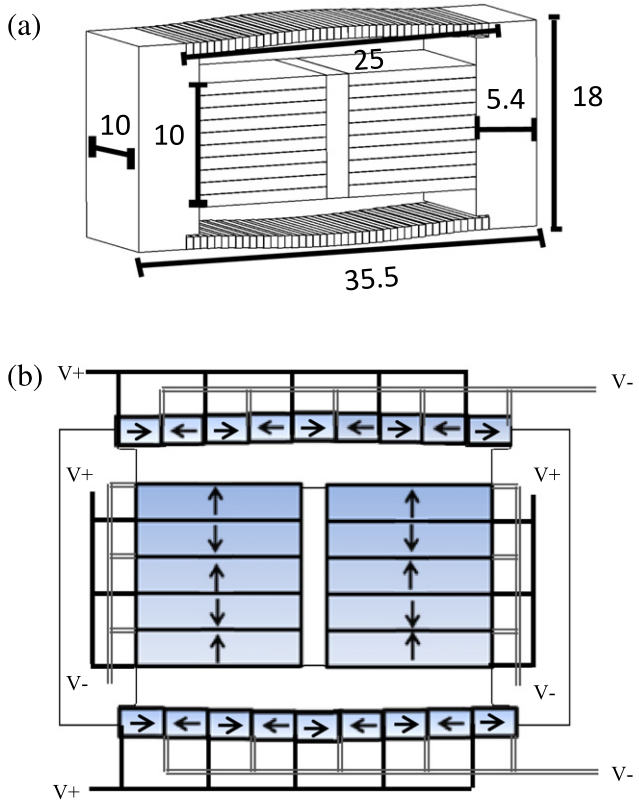

Figure 3. (a) Overall dimensions of stacked-HYBATS. All units are given in mm. (b) A reduced version of stacked-HYBATS is shown such that the poling directions (arrows) and voltage application are clearly visible. (c) Photograph of stacked-HYBATS.

Table 2. Dimensions of active materials in stacked-HYBATS.

Component	Number of piezoelectric plates	Thickness of each plate (mm)
Positive strain component	43	0.6
Negative strain component	20	1

The piezoelectric plates in each of the components are connected mechanically in series and electrically in parallel to produce the expansion and contraction described in section 2. Displacement measurements for both static and dynamic electric field application were taken using a laser vibrometer (Polytec, PI, Inc., model OFV-512) with a laser beam measuring 5 μm in diameter.

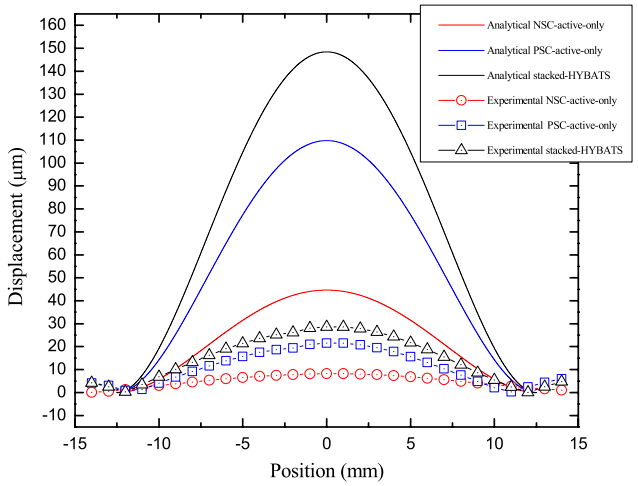

Figure 4. Analytical and experimental displacement profiles of stacked-HYBATS for each of the three displacement components under a 150 V_{DC} bias and 1 Hz 100 V_{rms}. Finite element modeling is necessary to resolve the discrepancy between the experimental and analytical results.

The displacement profiles generated analytically and experimentally by stacked-HYBATS at 150 V_{DC} and 1 Hz 100 V_{rms} are shown in figure 4. Experimental results showed that stacked-HYBATS has three displacement components: one activated by both the positive and negative strain components together, one activated by the positive strain component only, and one activated by the negative strain component only. The analytical displacement profile, $z_{\text{stacked–HYBATS}}(x)$, was found by calculating

$$z_{\text{stacked–HYBATS}}(x) = 2\,[z(x) - z_{\text{i}}(x)] \tag{3}$$

where $z_{\text{i}}(x)$ is the initial displacement profile of the device as given above and $z(x)$ is the deformed displacement profile of the device. The calculation of $z(x)$ is as follows. For a given voltage, the length of the negative strain component is found from

$$L = L_0\left(1 + \frac{L_{\text{e}}}{L_0} d_{31} E\right) \tag{4}$$

where L_0 is the non-deformed length of the negative strain component (NSC), L_{e} is the length of the active material in the NSC, d_{31} is the transverse piezoelectric coefficient of the active material in the NSC, and E is the applied electric field. Then, the curvature length of a deformed PSC can be calculated by using

$$L^{\text{d}}_{\text{PSC}} = L^{\text{i}}_{\text{PSC}}\left(1 + \frac{nt}{L^{\text{i}}_{\text{PSC}}} d_{33} E\right) \tag{5}$$

or

$$L^{\text{d}}_{\text{PSC}} = \int_{-L/2}^{L/2}\left[\left(\frac{\text{d}z_{\text{i}}(x)}{\text{d}x}\right)^2 + (1)^2\right]^{1/2} \text{d}x \tag{6}$$

where n is the number of piezoelectric plates in the stack, t is the thickness of the piezoelectric plates in the stack, and $z(x)$ is shown below in equation (7), a function of L and c (an

unknown).

$$z(x) = \frac{1}{c}\left[\left(\frac{L}{2}\right)^2 - x^2\right]^2. \tag{7}$$

Equation (8) is the result of combining equations (5)–(7). Substituting in values, we can solve for an updated c constant and obtain $z(x)$.

$$L^{\mathrm{i}}_{\mathrm{PSC}}\left(1 + \frac{nt}{L^{\mathrm{i}}_{\mathrm{PSC}}} d_{33}E\right) = \int_{-L/2}^{L/2} \sqrt{\frac{1}{c^2(4x^3 - L^2x)^2 + 1}}\,\mathrm{d}x. \tag{8}$$

The analytical results agree with the experimental results in that the analysis yields three distinct displacement components. However, the analytical results are five times greater than the experimental results. To this end, finite element modeling must be employed to verify the experimental results and provide insight into the difference between the experimental and analytical results.

4. Finite element modeling

4.1. Methods

In order to verify experimental and analytical results and compare stacked-HYBATS with commercial flextensional actuators, finite element modeling was conducted using ANSYS Workbench 12.1 and ANSYS mechanical applied parametric design language (MAPDL). The piezoelectric elements in the designs were modeled as SOLID226 elements with the 1001 KEYOPT activated. This is the most recently updated coupled-field element type available in ANSYS software. SOLID226 elements are 3D 20-node coupled-field hexahedra with nodes at each corner and at the midpoint of each edge. The mathematical functions corresponding to the active degrees of freedom at each node are quadratic; degrees of freedom for position in the x-, y-, and z-directions as well as for the electric potential were activated. Each electrode was modeled as an equipotential surface. The elasticity matrix, the piezoelectric matrix, and the permittivity matrix were specified in order to correctly model the active materials. A sample mesh used for the finite element modeling is shown below in figure 7.

4.2. Materials

Two different active materials were used to model the piezoelectric multilayer stacks (such as those shown in figure 1): NEPEC-N10 and TRS-HK1-HD [23]. NEPEC-N10 is a commercial PZT-5 material. TRS-HK1-HD is a newer material available from TRS Technologies and is a piezoceramic with very large electromechanical coupling coefficients. The properties of these materials are shown in table 3.

Table 3. Properties for piezoelectric materials used in simulations.

Property	Units	NEPEC-N10	TRS-HK1-HD
ρ	kg m^{-3}	8000	8000
d_{31}	m V^{-1}	-2.87×10^{-10}	-3.6×10^{-10}
d_{33}	m V^{-1}	6.35×10^{-10}	8.00×10^{-10}
d_{15}	m V^{-1}	9.3×10^{-10}	8.4×10^{-10}
s^{e}_{11}	m^2 N^{-1}	1.48×10^{-11}	1.54×10^{-11}
s^{e}_{33}	m^2 N^{-1}	1.81×10^{-11}	1.75×10^{-11}
s^{e}_{12}	m^2 N^{-1}	-5.03×10^{-12}	-4.6×10^{-12}
s^{e}_{13}	m^2 N^{-1}	-8.45×10^{-12}	-7.4×10^{-12}
s^{e}_{44}	m^2 N^{-1}	4.49×10^{-11}	2.16×10^{-11}
s^{e}_{66}	m^2 N^{-1}	4.49×10^{-11}	2.16×10^{-11}
K^T_{11}	—	5000	1600
K^T_{33}	—	5440	2500

Table 4. Properties of isotropic materials used in simulations.

Material	Young's modulus (GPa)	Poisson's ratio
Spring steel	210	0.283
Passive ceramic	27	0.34
Loctite Hysol Epoxy Resin RE2039	2.24	0.34
Brass	100	0.34

Passive ceramic, spring steel, brass, and Loctite Hysol Epoxy Resin are linear isotropic materials used in modeling the frame, electrodes, and bonding epoxy. The Young's modulus and Poisson's ratio for these materials were taken from materials databases. The properties of these materials are shown in table 4.

4.3. Boundary conditions

We investigated the static structural, modal, and harmonic responses of stacked-HYBATS in this study. Additionally, the blocking force of the stacked-HYBATS was calculated using finite element analysis. The boundary conditions for the various investigations are described below.

A quarter model of the geometry was used to determine the static displacement, natural frequency, resonant displacement, and blocking force of a given actuator configuration. This reduced the number of elements and nodes and minimized computation time. For these analyses, symmetry boundary conditions were placed on the surfaces corresponding to $x = 0$ and $y = 0$ as shown in figure 5. Such boundary conditions set out-of-plane translations and in-plane rotations to zero. In the results presented in this work, the vertical displacement profiles were found by measuring the vertical displacement at the edge of each layer of piezoelectric material. To report the overall vertical output displacement of an actuator, a single measurement was taken at the highest center element when voltage was applied. For blocking force measurements a static load was placed on the highest center element and increased until the output displacement of the actuator was zero. A diagram of these boundary conditions with measurement points is shown below in figure 5.

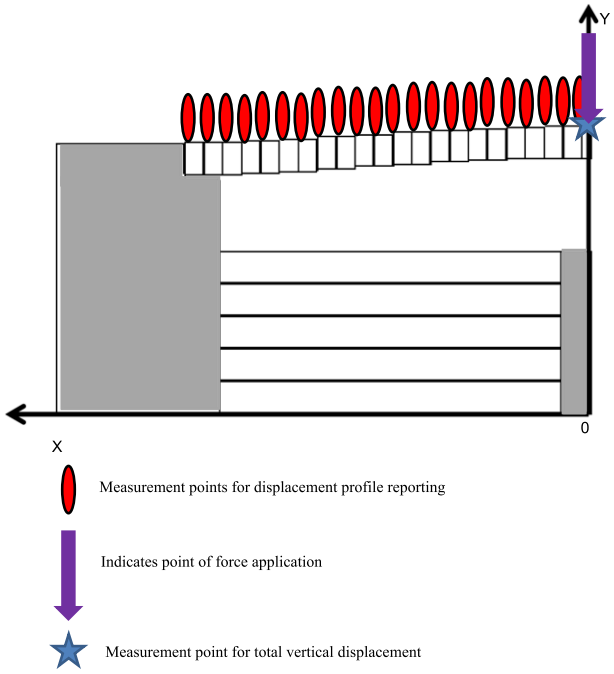

Figure 5. Quarter model of stacked-HYBATS. Gray areas are comprised of passive ceramic; white areas are comprised of piezoelectric material.

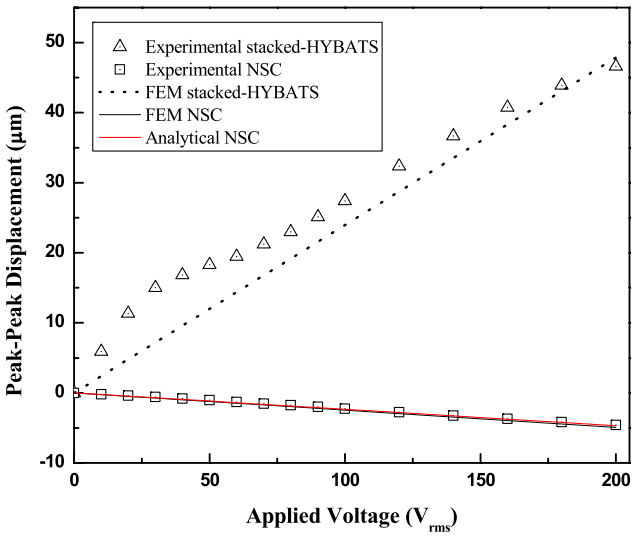

Figure 6. Comparison of experimental and modeled vertical displacement output for prototyped stacked-HYBATS and comparison of experimental, analytical, and modeled horizontal contraction for negative strain component in prototyped stacked-HYBATS.

4.4. Modeling assumptions for commercial flextensional actuator

The active component in the commercial flextensional actuator is a co-fired ceramic piezoelectric multilayer stack containing about 175 piezoelectric plates. The piezoelectric material was modeled as linear so the stack could be modeled as a piezoelectric brick instead of a design with separate layers. For example, the maximum displacement for a commercially available TOKIN multilayer stack actuator comprised of NEPEC-N10 is about 17 μm at the maximum operating voltage of 150 V_{DC}. The thickness of each layer in the stack was calculated to be 0.109 mm since the overall length of the stack was known. Finally, the applied DC voltage was used along with the thickness of the layers to determine the electric field applied to each layer of the stack. In the ANSYS simulations the voltage applied to the piezoelectric brick created the same electric field present in each of the layers of the stack.

5. Modeling results and discussion

5.1. Stacked-HYBATS modeling results

Stacked-HYBATS was modeled with dimensions as shown in figure 4. This simulation served multiple purposes. The first was to ensure the correctness of the boundary conditions used for modeling as described in section 4.3. The second was to examine the discrepancy between the analytical and experimental results published by Xu *et al* [23] in which the analytically modeled displacement was five times greater than the experimental displacement. An additional purpose of the modeling was to gain insight into the actuation mechanisms of all three displacement components. All of these results will benefit the future optimal designs of HYBATS.

Figure 6 shows a comparison between the experimental and finite element modeling results of the prototyped stacked-HYBATS. The device was biased with 150 V_{DC} and subjected to an AC voltage. This figure differs from figures 4 and 7 in that instead of obtaining the displacement profile for each point on the positive strain component (PSC), the total vertical output displacement of the device was measured at the point shown in figure 5 for increasing values of V_{rms}. Additionally, the total horizontal contraction of the negative strain component (NSC) was measured experimentally, and estimated analytically by using equation (4) and by FEM.

The experimental, analytical, and FEM measurements of the horizontal contraction of the negative strain component are in perfect agreement. This suggests that the flaw in the analytical modeling of stacked-HYBATS lies not in the calculation involving the NSC, but in the calculations related to the PSC. The FEM and experimental measurements of the combined effect of the positive and negative strain components differ somewhat, especially below $V_{rms} =$ 60. This can be attributed to the nonlinear behavior of the piezoelectric stack actuator in open-loop operation at low voltages which was not taken into account in the modeling [25]. The nonlinear effects are rather small and do not detract from the use of finite element analysis as a tool for the design and optimization of similar transducers.

Experimental results showed that stacked-HYBATS has three different displacement components. The experiment suggested that one displacement component can be activated by the synergetic contribution of the PSCs and NSC together, the second component by the activation of the PSCs alone, and the third component by the activation of the NSC alone. Figure 7 compares the experimental results with finite element

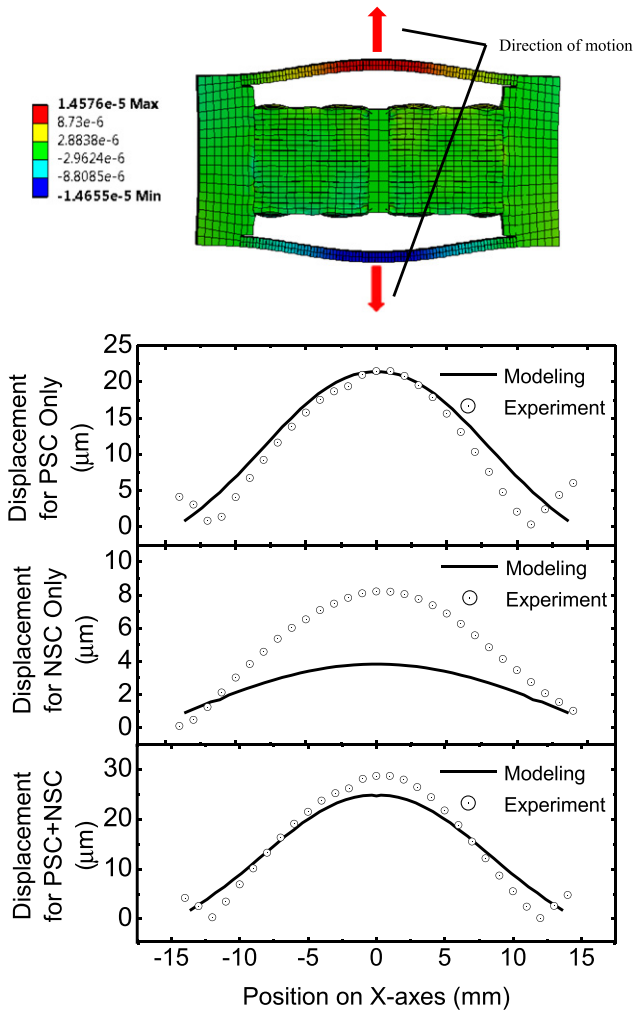

Figure 7. (Top) Deformed finite element model with arrows superimposed to show actuation direction. Displacement values shown are in meters. (Bottom) Comparison of ANSYS modeling and experimental results for the stacked-HYBATS. A driving voltage of 150 V_{DC} bias and 1 Hz 100 V_{rms} AC was used in the experiment and the simulation.

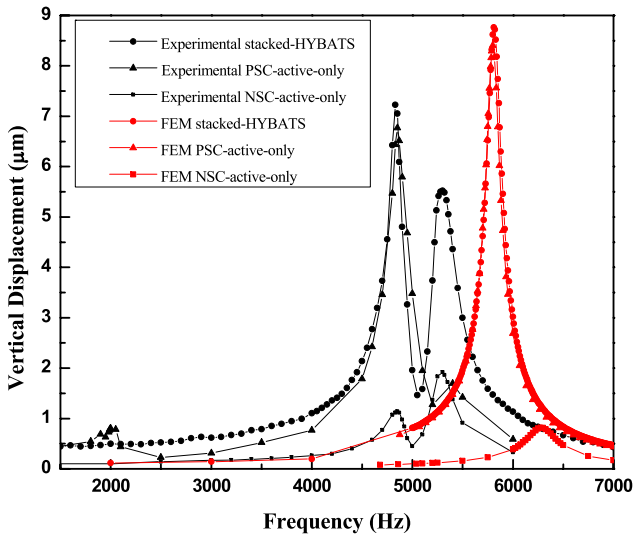

Figure 8. No-load harmonic response for the stacked-HYBATS, PSC-active-only mode, and NSC-active-only mode at 1 V_{rms} AC. Displacement in the vertical direction is plotted against the frequency of the AC driving signal.

modeling results and verifies that multiple displacement components are achievable with the device. The ANSYS results and the experimental results are in good agreement for the PSC activation. However, the modeled displacement results are less than the experimental results for the NSC activation as well as the simultaneous activation of the PSCs and NSC. Since the results in figure 6 show that the modeling of the negative strain component was in good agreement with the experimental and analytical results, we can conclude that the FEM underestimates the effect of the positive strain component when the negative strain component is activated. Thus, there must be some sort of interplay between the negative strain component and positive strain component when they are activated together that the modeling does not account for. One explanation is that the PSCs were more flexible in the experimental prototype than in the finite element model. This could be caused by relative motion or sliding between the active and passive components of this component, as suggested by Xu *et al* [23]. This presence of relative motion, sliding, or increased flexibility of the PSCs is supported by the experimental data. For the displacement component involving the simultaneous activation of the positive and negative strain components as well as the component involving positive strain only, the experimental results showed that the end of the actuator has a vertical displacement of up to 5 μm, and this displacement drops by 2–3 μm at a position about 10 mm from the actuator center before increasing again. The modeling and analytical results, however, showed a steady increase in displacement from the device end to the device middle. This suggests that the bonds in the prototyped PSCs are imperfect.

The experimentally determined resonance frequencies of each of the displacement components of the stacked-HYBATS [23] were compared with ANSYS modeling results for a no-load case. The NSC-active-only component and stacked-HYBATS each have two resonance peaks in the experimental results (4850 and 5300 Hz for the NSC-active-only mode and 4830 and 5300 Hz for the stacked-HYBATS) [23]. This is in contrast to the ANSYS modeling results where each component has only one resonance peak as shown in figure 8 (6300 Hz for the PSC-active-only mode, 6250 Hz for the NSC-active-only mode, and 5793 Hz for the stacked-HYBATS.) The additional resonance peaks in the experimental data could be due to asymmetry in the fabricated device [23]. The simulated device, however, was modeled to be symmetric about all three axes. Thus, we can expect that the modal analysis of the simulated device would yield only one resonance peak for each of the three modes. Comparison of the resonance frequencies between the experimental and simulated cases is difficult because of the multiple resonance peaks in the experimental case. However, a few observations are possible. In the simulated static analysis, any result involving the activation of the NSC underestimated the effect of the PSC. As one would expect,

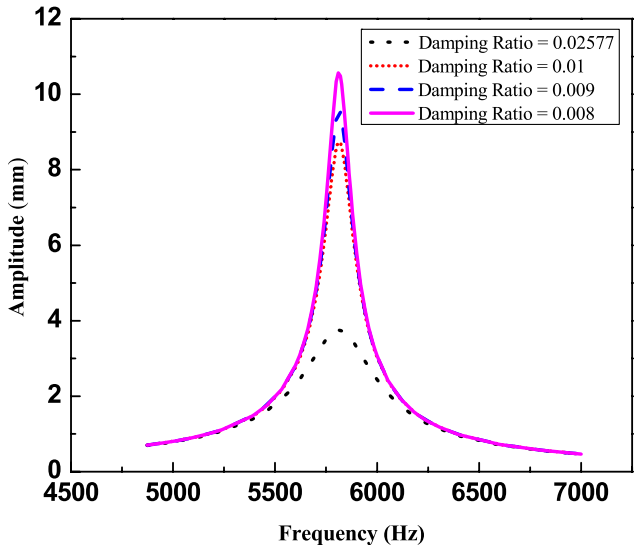

Figure 9. Harmonic response of stacked-HYBATS for damping ratios $\xi = 0.008, 0.009, 0.01, 0.025\,77$ at 1 V_{rms} AC.

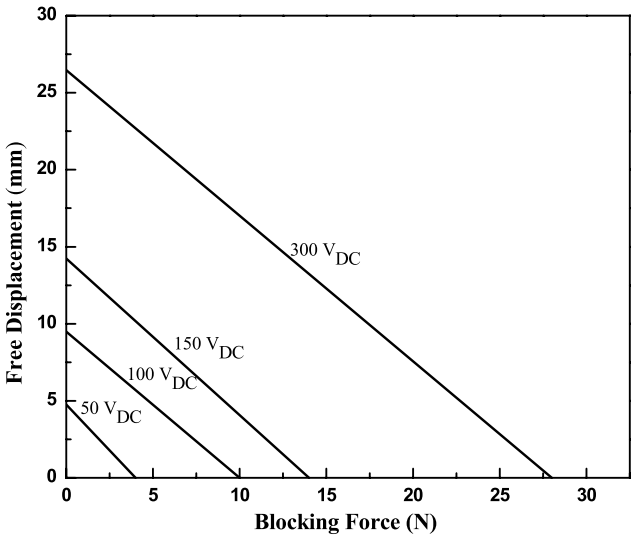

Figure 10. Free displacement versus blocking force curves for prototyped stacked-HYBATS. The coercive electric field, E_c, of TRS-HK1-HD is 500 V mm^{-1}; hence the maximum $V_{DC} = 300$.

the simulated resonant displacement of the NSC-active-only component is much smaller than its experimental counterpart. However, the displacement produced by the simulated negative strain component at resonance is 14.8 times as large as the displacement produced by this component at non-resonant frequencies. This same result is reported for the experimental stacked-HYBATS. Thus, even though the total displacement produced by stacked-HYBATS for the NSC-active-only component is underestimated, the ratio of the displacements at resonant and non-resonant frequencies is in good agreement with experimental results. This ratio of the resonant to non-resonant displacements is also true for the PSC and NSC active mode as well as the PSC-active-only mode and closely matches the experimental results. The simulation indicates that the effective piezoelectric coefficient of stacked-HYBATS is 3.1×10^6 pm V^{-1} at the resonance frequency.

As with all simulated dynamic analyses the effect of damping must be considered. The dielectric loss of the TRS-HK1-HD is small ($\tan\delta = 1.7\%$) and does not affect the resonant displacements at these frequencies. Thus, we turned our attention to viscous damping which is usually determined experimentally. In this case, however, experimental resonant displacements for stacked-HYBATS occurred at two different frequencies (at 4830 and 5300 Hz). Thus, it was difficult to extract accurate experimental values for damping. As an initial estimate the quality factor of the largest resonance peak in the experimental characterization of stacked-HYBATS was calculated. The quality factor (Q factor) is given by the following formula:

$$Q = \frac{f_r}{\Delta f} \tag{9}$$

where f_r is the resonance frequency of interest and $\Delta f = f_{high} - f_{low}$ where f_{high} and f_{low} are the two frequencies above and below the resonance frequency at which the displacement amplitude is half the resonant displacement. Then, the damping ratio can be calculated using

$$\xi = \frac{1}{2Q}. \tag{10}$$

Our initial estimate for the damping ratio calculated from (9) and (10) produced $\xi = 0.025\,77$ which was treated as frequency-dependent viscous damping in the finite element modeling. This damping ratio estimate resulted in an overdamped model as shown in figure 9. If the two resonant peaks in the experimental results were pulled together a higher Q factor would be obtained which would yield a smaller damping ratio. To illustrate how the device response changes as a function of damping ratio, the resonant displacement was simulated for a variety of damping ratios as shown in figure 9. A small variation in the damping ratio produces large variations in the displacement response at resonance. A damping ratio of $\xi = 0.01$ is a good fit for the experimental data.

Lastly, the blocking force of stacked-HYBATS was calculated using FEM. A static load was placed on the actuator as shown in figure 5. Voltage was applied to the actuator to determine the output displacement of the device with the static load in place. For a given voltage, the static load was increased until the vertical displacement of the actuator became zero. Figure 10 shows the displacement versus blocking force curves for the prototyped stacked-HYBATS. Commercial flextensional actuators are usually designed to maximize either free displacement or blocking force. Stacked-HYBATS, however, provides a good middle-of-the-road option in terms of both of these quantities. Additionally, this transducer has the advantage of being able to produce the same displacement and blocking force output but at a much lower voltage as long as the piezoelectric plates are made thinner, which is desirable in many applications.

Table 5. Device dimensions for comparative study.

Dimension	Length (mm)
w	28.7
h	13
d	5

5.2. *HYBATS versus flextensional actuators*

It is clear that stacked-HYBATS offers large displacements and strong resonance in a small footprint. To determine its commercial viability, however, stacked-HYBATS must be compared with a same-size commercially available flextensional actuator. Typical commercially available flextensional actuators feature a single piezoelectric multilayer stack made of PZT-5 operating in longitudinal mode. Since the strain induced in a piezoelectric material operating in longitudinal mode is about twice that of the material operating in transverse mode it is necessary to compare the stacked-HYBATS and flextensional actuators during operation in the same mode. Therefore, in this study three actuator configurations were compared: stacked-HYBATS, a d_{33} mode flextensional actuator, and a d_{31} mode flextensional actuator. The dimensions of each device were held constant as shown in table 5 and figure 11; each device was comprised of the same active material, NEPEC-N10. The frames of the flextensional actuators were composed of spring steel (as is typical commercially) while the end block of the updated stacked-HYBATS was composed of passive ceramic as in the experimental prototype [23]. The stacks in each device were taken to have a layer thickness of about 0.1 mm as in the commercial case. In this way, the electric field was equal in each of the piezoelectric layers in all three devices for proper comparison. The maximum stroke shown in figure 12 for stacked-HYBATS is about 141 μm while the maximum stroke for the d_{31} mode flextensional actuator is about 48 μm. Thus, we see that the maximum displacement output of the stacked-HYBATS design is almost 3 times greater than that of the d_{31} mode flextensional actuator. Additionally, as suggested in previous work [23], the modeling results show that the NSC-active-only stacked-HYBATS reduces to the case of the d_{31} flextensional actuator. When the piezoelectric plate thickness is held constant to compare the devices under an equal electric field the stacked-HYBATS outperforms a same-size d_{33} flextensional actuator by 15%. This margin could be increased by choosing appropriate curvature of the positive strain component.

For embedded active control applications it is necessary to examine the power consumption of the stacked-HYBATS as compared with the flextensional actuator. Under static operation, the power consumption is negligible for both actuators as the only power consumed is due to leakage current in the stacks. The power consumption that is present during operation under an AC field is the quantity that needs to be examined and is due to heat dissipation during the charging and discharging of the stacks. For a rough comparison the power can be given by

$$P \propto fCV^2 \tag{11}$$

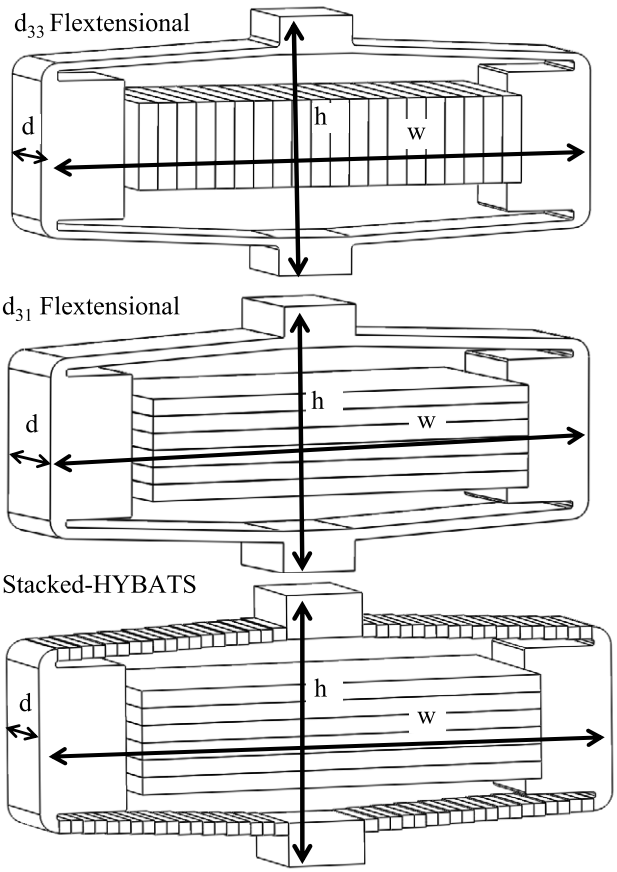

Figure 11. Diagram of the actuator geometry used for comparative study. The thickness of the plates shown in each device is exaggerated to show the device concept. In the comparative study, each plate of piezoelectric material had a thickness of 0.1 mm.

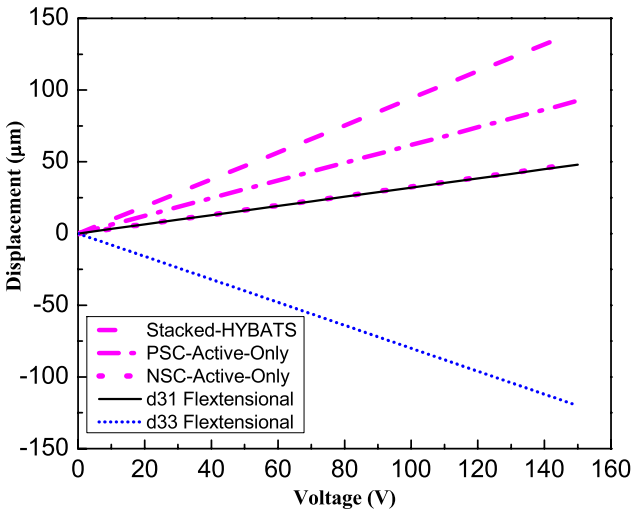

Figure 12. Vertical displacement versus DC voltage curve for stacked-HYBATS (long dash), a commercial flextensional actuator with a multilayer stack in d_{31} mode (solid black), and a commercial flextensional actuator with a multilayer stack in d_{33} mode (dots). The thickness of the piezoelectric plates in each component for all the devices was 0.1 mm. The maximum electric field in each device was 1.5 kV mm^{-1}.

Table 6. Comparison of power consumption per unit volume active material.

	Stacked-HYBATS	Flextensional
Volume of active material (mm^3)	1136.8	1000
Capacitance (μF)	4.97	3.87
Power consumption per unit volume of active material ($\mu W\ mm^{-3}$)	43.7	38.7

where f is the frequency of the AC field, C is the capacitance of the stack, and V is the applied voltage [26]. In the comparison of the flextensional actuator and stacked-HYBATS the thicknesses of the piezoelectric plates and the materials were held constant. This allows for a fair comparison of the transducers under the same voltage. Assuming that the frequency of the AC field applied to each transducer is equal, the power consumption becomes a function of the capacitance which can be calculated by using

$$C = n\frac{K_{33}^{T}\varepsilon_0 A}{t} \tag{12}$$

where n is the number of layers in the piezoelectric stack, ε_{33} is the dielectric constant of the material, A is the area of a single piezoelectric plate, and t is the distance between the electrodes. Table 6 shows the volume of the active material for each of the transducers, their calculated capacitances, and the power consumption per unit volume of active material calculated at 1 kHz and 100 V_{DC}. Stacked-HYBATS consumes 13% more power than the flextensional actuator but offers benefits in applications with its significant displacements, large blocking forces, and strong resonance.

6. Conclusion

Finite element modeling of a novel transduction structure, stacked-HYBATS, is presented in this paper. The FEM results are in good agreement with the experimental results reported in [23], in contrast to previously reported analytical results that were 5 times too large [23]. Modeling results show that stacked-HYBATS offers multiple displacement components, large output force, and strong resonance. These qualities benefit actuator applications which require large output displacement, accuracy on the micron scale, and relatively large output force in a very small package [27]. In terms of sensing and energy harvesting, stacked-HYBATS is superior to its flextensional counterpart because passive material is replaced with active material which allows for better transduction in a smaller footprint. Additionally, stacked-HYBATS surpasses transverse mode flextensional actuators in terms of displacement by a factor of 3 and longitudinal mode flextensional actuators by a factor of 1.15. Finite element analysis has proven to be a valuable tool for the evaluation of our novel device. Future generations of stacked-HYBATS will benefit from design and optimization by FEM.

References

[1] Li D, Wu M, Oyang P and Xu X 2006 Cymbal piezoelectric composite underwater acoustic transducer *Ultrasonics* **44** 685–7

[2] Michlmayr G, Cohen D and Or D 2012 Sources and characteristics of acoustic emissions from mechanically stressed geological data—a review *Earth-Sci. Rev.* **112** 97–114

[3] Sharapov V 2011 *Piezoceramic Sensors* (New York: Springer)

[4] Langenberg K, Marklein R and Mayer K 2012 *Ultrasonic Nondestructive Testing of Materials: Theoretical Foundations* (Boca Raton, FL: Taylor & Francis)

[5] Uchino K 1997 *Piezoelectric Actuators and Ultrasonic Motors* (Boston, MA: Kluwer Academic)

[6] Gaudenzi P 2009 *Smart Structures: Physical Behaviour, Mathematical Modelling and Applications* (Chichester: Wiley)

[7] Tressler J, Alkoy S and Newnham R 1998 Piezoelectric sensors and sensor materials *J. Electroceram.* **2** 257–72

[8] Wang Q, Zhang Q, Xu B, Liu R and Cross L 1999 Nonlinear piezoelectric behavior of ceramic bending mode actuators under strong electric fields *J. Appl. Phys.* **86** 3352–60

[9] Wolff A, Cramer D, Hellebrand H, Probst I and Lubitz K 1994 Optical two channel elongation measurement of PZT piezoelectric multilayer stack actuators *Proc. 9th IEEE Int. Symp. on Applications of Ferroelectrics (University Park, PA)* pp 755–7

[10] Wise S A 1998 Displacement properties of RAINBOW and THUNDER piezoelectric actuators *Sensors Actuators* A **69** 33–8

[11] Onitsuka K, Dogan A, Tressler J, Xu Q, Yoshikawa S and Newnham R 1995 Metal–ceramic composite transducer, the 'Moonie' *J. Intell. Mater. Syst. Struct.* **6** 447–55

[12] Dogan A, Uchino K and Newnham R 1997 Composite piezoelectric transducer with truncated conical endcaps Cymbal *IEEE Trans. Ultrason. Ferroelectr. Freq. Control* **44** 597–605

[13] Micromechatronics, Inc. 2012 http://www.mmech.com/cedrat-actuators/apa-overview/apasspecifications#APA1000XL1 (accessed on: December 2012)

[14] Xu T-B, Tolliver L, Jiang X and Su J 2013 A single crystal lead magnesium niobate–lead titanate multilayer-stacked cryogenic flextensional actuator *Appl. Phys. Lett.* **102** 042906

[15] Piezo Systems, Inc. 2012 http://www.piezo.com/prodbm7qm.html (accessed on: 6 December 2012)

[16] Micromechatronics, Inc. 2012 http://www.mmech.com/tokin-actuators/ned-tokin-resin-coated (accessed on: 6 December 2012)

[17] Marouze J P and Cheng L 2002 A feasibility study of active vibration isolation using THUNDER actuators *Smart Mater. Struct.* **11** 854–62

[18] Garcia-Bonito J, Brennan M J, Elliott S J, David A and Pinnington R J 1998 A novel high-displacement piezoelectric actuator for active vibration control *Smart Mater. Struct.* **7** 31–42

[19] Onitsuka K, Dogan A, Xu Q, Yoshikawa S and Newnham R 1994 Design optimization for metal–ceramic actuator, 'Moonie' *Ferroelectrics* **156** 37–42

[20] Fernandez J F, Dogan A, Fielding J T, Uchino K and Newnham R E 1998 Tailoring the performance of ceramic–metal piezocomposite actuators, 'cymbals' *Sensors Actuators* A **65** 228–37

[21] Micromechatronics, Inc. 2012 http://www.mmech.com/cedrat-actuators/apa-overview/apas-specifications#APA35XS (accessed on: 6 December 2012)

[22] Xu T-B and Su J 2005 Theoretical modeling of electroactive polymer–ceramic hybrid actuation systems *J. Appl. Phys.* **97** 0349081

[23] Xu T-B, Jiang X and Su J 2011 A piezoelectric multilayer-stacked hybrid actuation/transduction system *Appl. Phys. Lett.* **98** 2435031

[24] Su J, Xu T-B, Zhang S, Shrout T and Zhang Q 2004 An electroactive polymer–ceramic hybrid actuation system for enhanced electromechanical performance *Appl. Phys. Lett.* **85** 1045–7

[25] Goldfarb M and Celanovic N 1996 Behavioral implications of piezoelectric stack actuators for control of micromanipulation *Proc. IEEE Int. Conf. on Robotics and Automation (Minneapolis, Minnesota)* vol 1, pp 226–31

[26] Kawakita S, Isogai T, Ohya N and Kawahara N 1997 Multi-layered piezoelectric bimorph actuator *Proc. Int. Symposium on Micromechatronics and Human Science* pp 73–8

[27] Liu Y T and Higuchi T 2001 Precision positioning device utilizing impact force of combined piezo-pneumatic actuator *IEEE/ASME Trans. Mechatron.* **6** 467–73